ELSEVIER
Available online at www.sciencedirect.com
ScienceDirect
Earth and Planetary Science Letters xx (2008) xxx–xxx
EPSL
www.elsevier.com/locate/epsl

The great Sumatra–Andaman earthquakes — Imaging the boundary between the ruptures of the great 2004 and 2005 earthquakes

Dieter Franke [a,*], Michael Schnabel [a], Stefan Ladage [a], David R. Tappin [b], Soenke Neben [a], Yusuf S. Djajadihardja [c], Christian Müller [a], Heidrun Kopp [d], Christoph Gaedicke [a]

[a] *Federal Institute for Geosciences and Natural Resources (BGR), Stilleweg 2, 30655 Hannover, Germany*
[b] *British Geological Survey, Kingsley Dunham Centre, Keyworth, Nottingham, NG12 5GG, United Kingdom*
[c] *Agency for the Assessment & Application of Technology (BPPT), Jl. M.H. Thamrin no. 8, Jakarta 10340, Indonesia*
[d] *IFM-Geomar, Wischhoffstr. 1-3, Kiel, Germany*

Received 27 April 2007; received in revised form 28 January 2008; accepted 28 January 2008

Editor: R.D. van der Hilst

Abstract

Segmentation along convergent margins controls earthquake magnitude and location, but the physical causes of segment boundaries, and their impact on earthquake rupture dynamics, are still poorly understood. One aspect of the 2004 and 2005 great Sumatra–Andaman earthquakes is their abrupt termination along a common boundary. This has led to speculation on the nature of the boundary, its origin and why it was not breached.

For the first time the boundary has been imaged and, with newly acquired marine geophysical data, we demonstrate that a ridge on the subducting Indo-Australian oceanic crust may exert a control on margin segmentation. This suggests a lower plate influence on margin structure, particularly its segmentation. The ridge is masked by the sedimentary cover in the trench. Its most likely trend is NNE–SSW. It is interpreted as a fracture zone on the subducting oceanic plate. A ramp or tear along the eastern flank of the subducting fracture zone beneath Simeulue Island may be considered as intensification factor in terms of rupture propagation barrier.

Keywords: subduction; earthquakes; segmentation; seismic data; Sumatra

1. Introduction

Rupture propagation during earthquakes along convergent margins may commonly be confined to discrete along-strike structural segments. However, it is recognised that rupture propagation across such segment boundaries can result in megathrust earthquakes of considerable destructive power that may generate transoceanic tsunami. The control on earthquake propagation exerted by segment boundaries is well established (Spence, 1977; Ando, 1975) but the physical causes are poorly understood. As a result we cannot fully determine seismic and tsunami hazard along convergent margins globally. Several mechanisms are recognised as influencing segmentation. These include: discontinuities in the geometry of the subducting plate such as slab tears (Spence, 1977; Aki, 1979); topographic anomalies within the subducting plate, such as ridges, fracture zones and seamount chains (Kodaira et al., 2000; Cummins et al., 2002; Bilek et al., 2003; Collot et al., 2004), major structures crossing the over-riding plate (Ryan and Scholl, 1993; Collot et al., 2004) and large-scale variations in the buoyancy of the subducting plate related to its thermal age (Yáñez and Cembrano, 2004).

In the instance of the great Indian Ocean earthquakes of 2004–5 the southern boundary of the December 26th 2004 event is clearly delineated (e.g. Ammon et al., 2005; Bilham, 2005; Krüger and Ohrnberger, 2005; Lay et al., 2005; Gahalaut et al., 2006). Significantly, this boundary also delineates the northern termination of the March 28th 2005 earthquake (e.g.

* Corresponding author. Tel.: +49 511 643 3235; fax: +49 511 643 3663.
E-mail address: Dieter.Franke@bgr.de (D. Franke).

0012-821X/$ - see front matter
doi:10.1016/j.epsl.2008.01.047

Please cite this article as: Franke, D., et al., The great Sumatra–Andaman earthquakes — Imaging the boundary between the ruptures of the great 2004 and 2005 earthquakes, Earth Planet. Sci. Lett. (2008), doi:10.1016/j.epsl.2008.01.047

Ammon, 2006; Subarya et al., 2006). A large-scale structure near Simeulue Island (Fig. 1) has been suggested as a control on the ruptures, but its specific nature is unknown. Singh et al. (2005) and Kamesh Raju et al. (2007) propose an upper plate control on the segment boundary with the West Andaman Fault as a key structure controlling rupture propagation. DeShon et al. (2005) propose that the boundary of the southern Andaman microplate, in the vicinity of Simeulue Island is a diffuse deformation zone, and that this developing plate boundary served as a barrier to rupture propagation. Dewey et al. (2007) propose a lower plate control, suggesting that a distortion of the plate interface at depth beneath the forearc may be the cause. More specifically, Subarya et al. (2006) suggest that a boundary has formed due to distortion of the plate interface, related to a north–south trending fracture zone on the incoming oceanic plate.

The aim of this study, therefore, is to characterize the plate interface and structural architecture in the vicinity of the segment boundary between the December 26th 2004 and March 28th 2005 mainshocks. To this end, during 2006, we acquired swath bathymetry, multichannel reflection seismic (MCS), and wide-angle/refraction seismic data. Along trench-parallel profiles these data image the oceanic plate subducting beneath the forearc as well as upper plate structures. On the oceanic plate there is a broad N–S trending ridge entering the accretionary wedge SW of Simeulue. The influence of this ridge on segmentation of the upper plate is discussed.

2. Tectonic setting

Along the convergent margin off Sumatra the oceanic Indo-Australian Plate subducts under the Eurasian Plate (Fig. 1). As the former plate moves northward, convergence becomes increasingly oblique from south to north. In the vicinity of the December 2004 epicentre the azimuth of convergence is N10°E at 4°N, 95°E, (Delescluse and Chamot-Rooke, 2007). The result is large-scale strain partitioning with trench-normal and trench-parallel shear components. Along the leading edge of the Eurasian Plate, the trench-parallel shear results in large-scale, dextral strike-slip fault systems within the forearc basins and on Sumatra. Along the plate margin continental sliver plates have formed (Malod and Kemal, 1996; Simandjuntak and Barber,

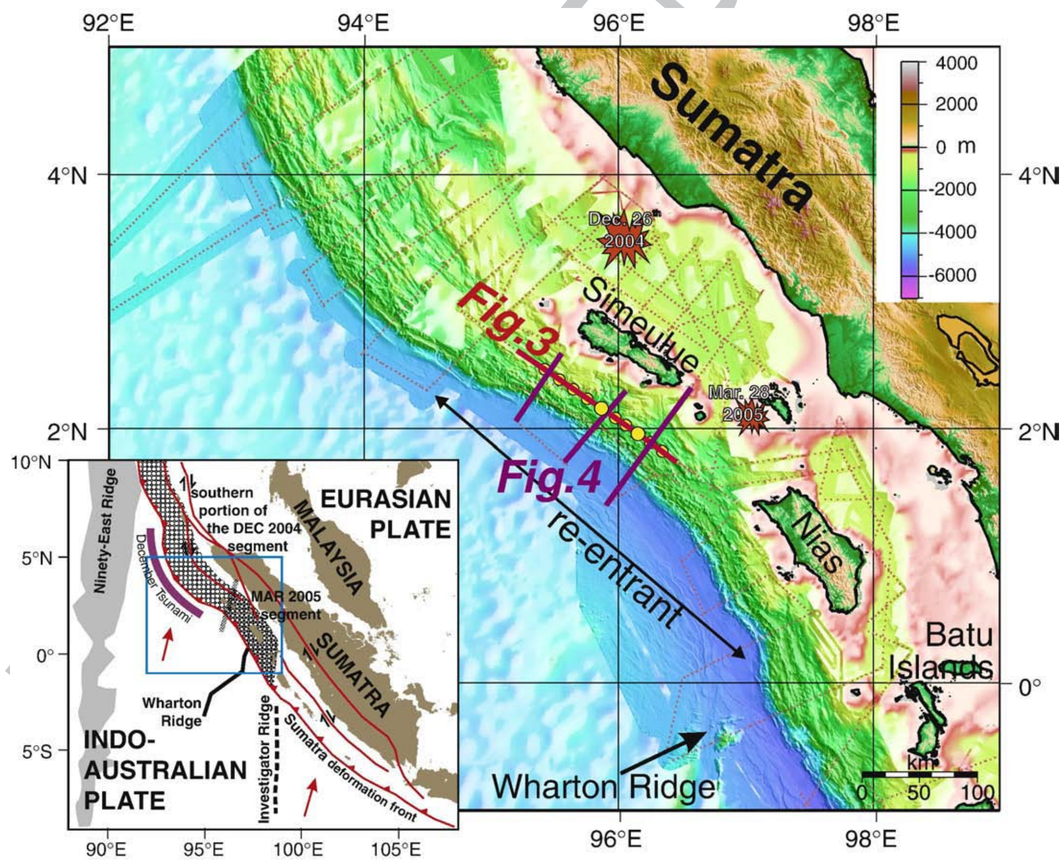

Fig. 1. Bathymetry off Sumatra underlain by satellite altimetry (Smith and Sandwell, 1997). Yellow dots mark positions of ocean-bottom hydrophone/seismometer stations and enlarged the two example stations shown in Fig. 2. Light red dashed lines give location of MCS profiles acquired during RV Sonne cruises and thick red and purple lines indicate location of multichannel seismic profile shown in Figs. 3 and 4, respectively. The locations of the initiation of rupture of the December 26th 2004 and March 28th 2005 great Sumatra–Andaman earthquakes are indicated. The only striking feature entering the subduction zone is the extinct Wharton spreading ridge southwest of Nias Island. The inset shows the tectonic situation with the Sumatra deformation front (red line with teeth) and major structures on- and offshore. The red arrows indicate the convergence direction of the Indo-Australian and Eurasian plates. The December 2004 and March 2005 rupture zones are indicated by different shades. The location of major structures on the Indo-Australian oceanic plate as the Ninetyeast, Wharton and Investigator ridges are indicated. (For interpretation of the references to colour in this figure legend, the reader is referred to the web version of this article.)

Please cite this article as: Franke, D., et al., The great Sumatra–Andaman earthquakes — Imaging the boundary between the ruptures of the great 2004 and 2005 earthquakes, Earth Planet. Sci. Lett. (2008), doi:10.1016/j.epsl.2008.01.047

1996; McCarthy and Elders, 1997; Baroux et al., 1998; Sieh and Natawidjaja, 2000).

Off central Sumatra the convergent margin is mainly linear (Fig. 1), but farther north, in the region of the December 2004 and to the March 2005 ruptures, it becomes markedly arcuate along an area we here term the ‘re-entrant’ (Fig. 1). Northwest of the re-entrant a change in morphology and structure of both the accretionary prism and the oceanic plate takes place. To the northwest, the Sumatra deformation front continues as a salient, with its apex offset ~150 km to the west (Henstock et al., 2006; Fig. 1). The outboard slope of the accretionary prism is a pronounced feature with steep gradients of approximately 4° to 8° passing from 4500 m at the base to 1500 m at the top, where it forms an irregular plateau with water depths as shallow as 200 m. There is no distinct outer arc high. The accretionary prism is 140 km wide with a structural trend generally parallel to the margin (Sibuet et al., 2007). At the re-entrant the architecture of the March 2005 rupture segment, is remarkably different to that in the north. The width of the accretionary prism decreases to 100 km (from the deformation front to the West Andaman fault), the wide plateau seen in the north disappears, and the more usual tapered form of an accretionary prism is present. There is an outer arc high on which are located a chain of small islands, of which Simeulue is the most northerly (Fig. 1). The region between Nias and Simeulue islands forms a broad northeast facing re-entrant.

3. Methodology

3.1. Wide-angle/refraction seismics

To obtain reliable velocity and structural information on the deeper section of the accretionary wedge we acquired wide-angle/refraction seismic data along two MCS profiles; BGR06-208a and BGR06-135 (Fig. 1). Line BGR06-208a is situated southwest of Simeulue Island. It is parallel to the trench and at a mean distance of about 34±2 km from the toe of the accretionary prism. Along this line, ten ocean-bottom hydrophones/seismometers were deployed with a mean separation of 15 km (Fig. 1). 1763 shots were fired at intervals of about 106 m, resulting in a total length of profile of 186 km. The wide-angle seismic instruments recorded energy from an offset range of at least −60 to 60 km (see Fig. 2 and Supplements 1 and 2 in Appendix A). At all 10 stations we recorded well defined refracted waves from within the sedimentary column (Pg) of the accretionary prism as well as clear wide-angle reflections of the subducting oceanic crust (PcP).

We constructed velocity–depth models by applying a tomographic method — tomo2d, (Korenaga et al., 2000) which inverts traveltimes from both refracted and reflected waves. The result is a velocity–depth-distribution and the position of the seismic reflection from the subducted oceanic crust. The modelling sequence for line BGR06-208a is as follows. For the compilation

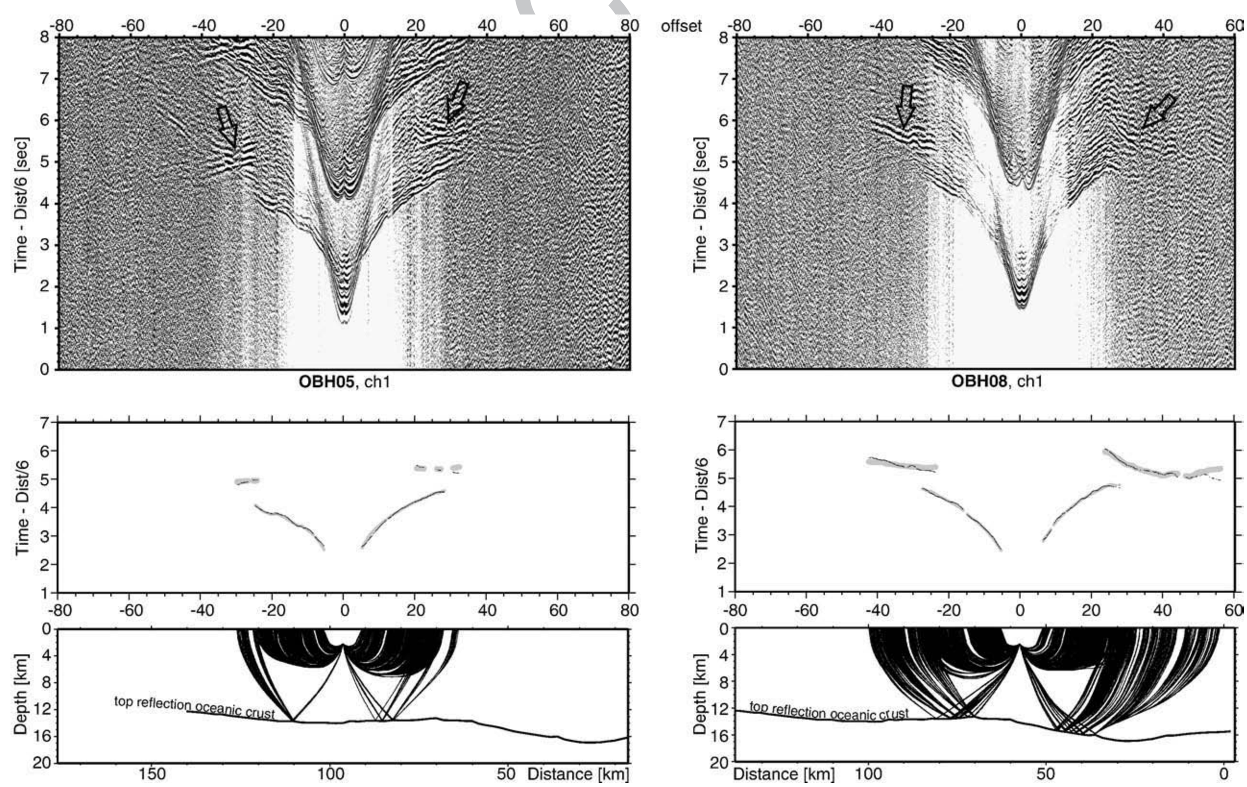

Fig. 2. Two example seismic sections from ocean-bottom stations (top), observed and calculated traveltimes (middle) and rays corresponding to the calculated traveltimes (bottom). The profile kilometre scale (Distance) corresponds to that of Fig. 3 while the offset scale is referring to the shot-receiver distance. OBH05 (left) is located above the flat lying oceanic crust while OBH08 (right) is located above a depth step of the oceanic crust. A major difference in the wide-angle reflection from the top oceanic crust is distinct in the seismogram (see arrows). The location of the two stations is marked in Fig. 1 as enlarged yellow dots. Seismograms, calculated rays and traveltimes of all remaining eight stations are shown in Supplements 1 and 2 in Appendix A.

Please cite this article as: Franke, D., et al., The great Sumatra–Andaman earthquakes — Imaging the boundary between the ruptures of the great 2004 and 2005 earthquakes, Earth Planet. Sci. Lett. (2008), doi:10.1016/j.epsl.2008.01.047

of the starting model, we constrained the depth of the sea bottom with bathymetric data and used a 1-D velocity model with a constant gradient along the whole profile. The inversion was run in two steps. Firstly, inversion of the refracted waves through the sedimentary column provided a detailed velocity–depth model of the upper 6 to 8 km below sealevel. Between these depths the refracted waves, calculated as diving waves, reached their turning point and travelled back to the surface. Secondly, the traveltimes for reflected waves were calculated. The results provide both the seismic velocities between the well-constrained upper sedimentary section and the top of the oceanic crust at a depth of about 12 to 16 km together with the depth and profile of the oceanic crust. The top oceanic crust reflection is shown in Fig. 3 only for those regions where there is a good coverage of seismic rays, where the location of crust is well constrained.

The RMS misfit of the PcP phases is in the range of accuracy by which the traveltimes of the PcP phases could be picked. This misfit is less than 100 ms and gives an error in the depth determination of the oceanic crust reflector of less than 300 m. The traveltimes of the Pg-phases are better resolved than those from the PcP, with a misfit of less than 40 ms. From these results we consider the velocity model and depth to the oceanic crust to be well defined.

To confirm that the structures imaged are within the spatial resolution of the data, we performed checkerboard tests (Supplement 3 in Appendix A). The final velocity model, as obtained by the tomography, was tested with superimposed velocity anomalies of systematically decreasing size. A set of first arrival times and reflection phases together with corresponding ray paths were generated and formed the input for another tomography using the given source–receiver configuration. If the perturbed model can be reproduced by the tomography the size of the velocity anomalies are within the vertical and horizontal resolution of the data. In this way we are able to resolve velocity variations with a dimension of less than 20×8 km. At the southeastern end of line BGR06-208a, the top oceanic crust reflector is more than 3 km deeper than in the centre of the profile (Fig. 3). The deeper location of the top oceanic crust reflector was found over a distance of 40 km, i.e. twice the horizontal resolution of better than 20 km. This proves that the depth change identified is not a velocity artefact caused by variations in the overlying sedimentary sequence. In fact there is a uniform velocity structure in the sediments resting on the subducting oceanic crust (Fig. 3). A constant depth for the subducting oceanic crust would only be possible if there was a distinct, and very large, low velocity zone (i.e. a very strong velocity inversion) in the sediments above the section where we identify the deeper oceanic crust (profile km 0–70). Such an inversion is not possible.

To address the question of velocity–depth ambiguity, we systematically varied the depth kernel weighting parameter (Korenaga et al., 2000). The final velocity model shown in Fig. 3 was calculated with a weighting parameter of unity, which corresponds to equal weighting of velocity and depth nodes. Decreasing the weighting parameter should lead to smaller depth variations with larger velocity variations. However, even with an implausible kernel weighting parameter as small as 0.1 (where the velocity perturbations are very much greater than the perturbation of the depth of the resulting reflector), the top of the oceanic crust in the final model shows a depth change of 2 km towards the southeast.

The second wide-angle/refraction seismic line BGR06-135 runs perpendicular to the trench in SW–NE direction. The line

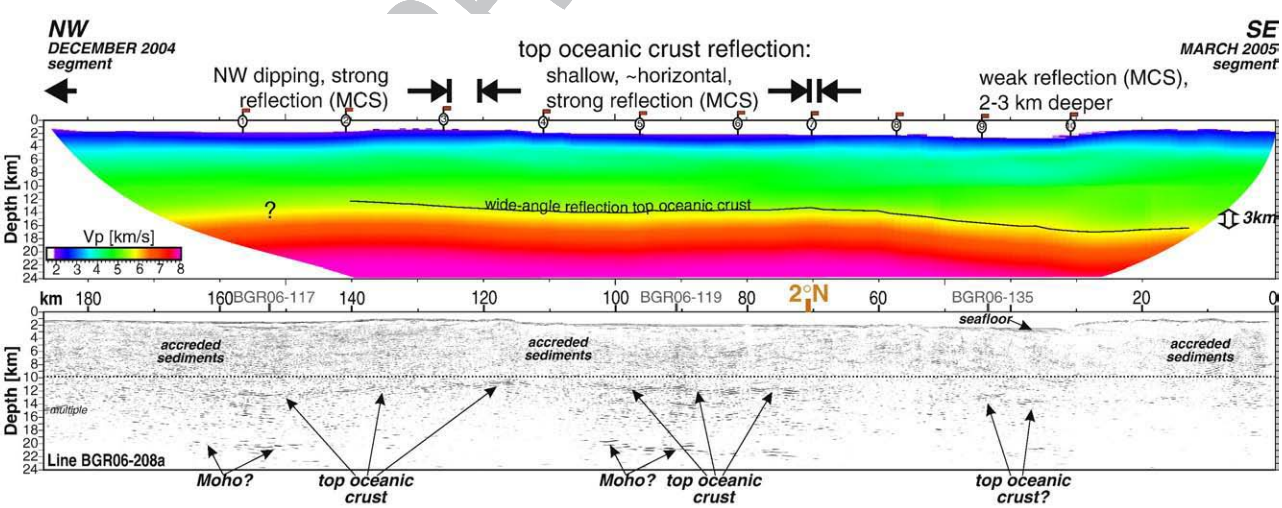

Fig. 3. Velocity–depth model (top) as derived from wide-angle/refraction seismic data and a prestack-depth migrated multichannel seismic line (bottom). Line BGR06-208a runs margin parallel from the December 2004 segment across the segment boundary and extending SE-ward on the March 2005 segment. The location of the profile is indicated as thick red line in Fig. 1. Top: The inversion of the refracted waves from 10 ocean-bottom stations revealed a detailed velocity–depth model of the model's upper 6 to 8 km. The traveltimes from reflected waves gave a detailed image of the seismic velocities down to the top of the oceanic crust at a depth of about 12 to 16 km. We resolve the shape of the subducting oceanic plate along the profile (black line). In the SE (km 70 to 15) a distinct depth step of the subducting oceanic crust of more than 3 km is resolved. Bottom: The top reflection from the subducting oceanic crust is well imaged north of 2°N (profile km 160–70). It shows a dip to the NW from about 11 km depth to 12.5 km depth (profile km 120 to 160). The reflection vanishes at the NW end of the line, where the initial velocity model for depth migration is poorly controlled. In the centre of the line (profile km 70–120) the strong reflective top of the oceanic crust lies continuously at a shallow depth of 11 to 12 km. Southeast of 2°N (profile km 70–20) only weak reflections are visible, which are located at 2 to 3 km greater depth.

extends for 215 km from the oceanic plate to the Simeulue forearc basin. We recorded at a total of 31 ocean-bottom stations. Due to higher ships speed a shooting interval of 60 s resulted in an average shot spacing of about 120 m. Here we only concentrate on the western, seaward, part of the line and use traveltimes of refracted waves from 13 stations to derive the velocity–depth model. PcP phases from 5 stations constrain velocities at greater depth down to the subducting oceanic crust.

We used a similar modelling procedure for this wide-angle/refraction line as for line BGR06-208a. The resulting model provides seismic velocities for the trench fill and for the accretionary prism up to 60 km landward of the prism toe. The prism sediments have values of 4.0 km/s at a depth of 3 km below seafloor, and reach a value of 5.5 km/s at about 13 km below seafloor.

The results from the two wide-angle/refraction seismic lines provided an initial velocity model for the depth migration of the MCS lines (Section 3.2). Reflections beneath the top oceanic crust were recorded only occasionally in the wide-angle data. Thus the deeper parts of the velocity model are based mainly on extrapolation and, therefore, are tentative. In the MCS processing, in order to avoid any migration artefacts, we smoothed these velocity models in the crustal area with a vertical window of 3 km. Thus there are minor differences between the wide-angle and the MCS velocity models.

3.2. Multichannel reflection seismics (MCS)

During our marine surveys over the 2004 and 2005 rupture zones a comprehensive dataset of some 9000 line kilometres of MCS data were acquired together with gravity and magnetics data. MCS data were acquired with a 240 channel, 3 km streamer (offset to near group: 150 m; maximum offset: 3,137.5 m), and a tuned airgun array comprising 16 airguns with a total capacity of 50.8 L. Record length was 14 s with a sample interval of 2 ms. A shot interval of 50 m resulted in a fold of 30.

Processing of four MCS lines was performed up to full Kirchhoff prestack-depth migration and included the production and correction via MVA (migration velocity analysis) of a depth velocity model. After testing various combinations of processing parameters the following sequence was regarded as optimal. Prestack processing included geometry editing, deconvolution, true amplitude recovery, and filtering. Reduction of water-bottom multiples (a major challenge) was achieved by applying a parabolic radon filter and inner trace mutes. Stacking velocities, at an average distance interval of 3 km, were determined for the reference poststack time migrated sections. The initial depth model was derived from the wide-angle/refraction seismic data along the lines BGR06-135 and BGR06-208a and from smoothed DMO velocities, adjusted and calibrated at the cross point with the refraction seismic line for lines BGR06-117 and -119. The upper parts of the velocity fields were iteratively improved via MVA until the migrated CRP gathers were flat. Quality control included a detailed evaluation of congruence between the poststack migrated sections and the time-converted prestack-depth migrated sections. Kirchhoff time migration, based on smoothed interval velocities derived from stacking velocities, completed the poststack migration sequence for the reference time migrated lines as well as for the additional lines not depth migrated. Finally, time and space variant signal filtering, time varying scaling and, along some sections, a smooth fx-deconvolution completed the poststack processing sequence.

3.3. Bathymetry

Swath bathymetry was acquired by the RV Sonne using a 12 kHz Simrad EM 120 and by the HMS Scott using 12 kHz SASS-IV system (Henstock et al., 2006, Ladage et al., 2006). The swath data was compiled and merged to provide a complete map of the area off northern Sumatra (Figs. 1 and 6). Interpretations of the swath bathymetry were integrated with geodetic data to provide an overall picture of the structure of the boundary between the 2004/2005 earthquakes located in the vicinity of Simeulue Island.

4. Results

4.1. Image of the plate interface

The margin-parallel line BGR06-208a (Fig. 3) crosses the boundary between the two earthquake ruptures of 2004 and 2005 in the vicinity of Simeulue Island. It lies 34±2 km landward of the deformation front. From the wide-angle seismic data the velocity–depth model resolves the top oceanic crust between line kilometres 15 and 140 (Fig. 3 — top). Only at the margins is the ray coverage insufficient to image the reflection. The oceanic crust is subhorizontal at a depth of about 12 km along the central part of the line. To the southeast over a distance of 40 km the ocean crust depth gradually increases in depth by more than 3 km (Fig. 3 — top; profile km 60–20; south of 2°N). Since the velocities of the overlying, accreted sediments are uniform along the line the depth change is not an artefact due to velocity pull-down.

The MCS data provides complementary insights into the finer detail of the sedimentary prism, together with the crustal structure than available from the wide-angle seismic data. Reflections of the sedimentary prism and the underlying oceanic crust allow refinement of the coarse interpretations based on the refraction results. Conversely, the refraction models provide a constraint on interpretations of the MCS (Mooney and Brocher, 1987).

On the MCS data, the profile of the subducting oceanic crust is seen to be broadly similar to that on the wide-angle seismics (Fig. 3 — bottom). However, there are distinct regions of strongly reflective oceanic crust alternating with regions of weaker reflections. In the centre of the line (Fig. 3 — bottom; profile km 70–120) the strongly reflective top of the oceanic crust lies continuously at a shallow depth of 11 to 12 km. To the northwest the strongly reflective oceanic crust dips slightly from about 11 km to 12.5 km depth (Fig. 3 — bottom; profile km 120 to 160). The oceanic crust reflection is not imaged at the northwestern end of the line where the initial velocity model for depth migration is poorly controlled.

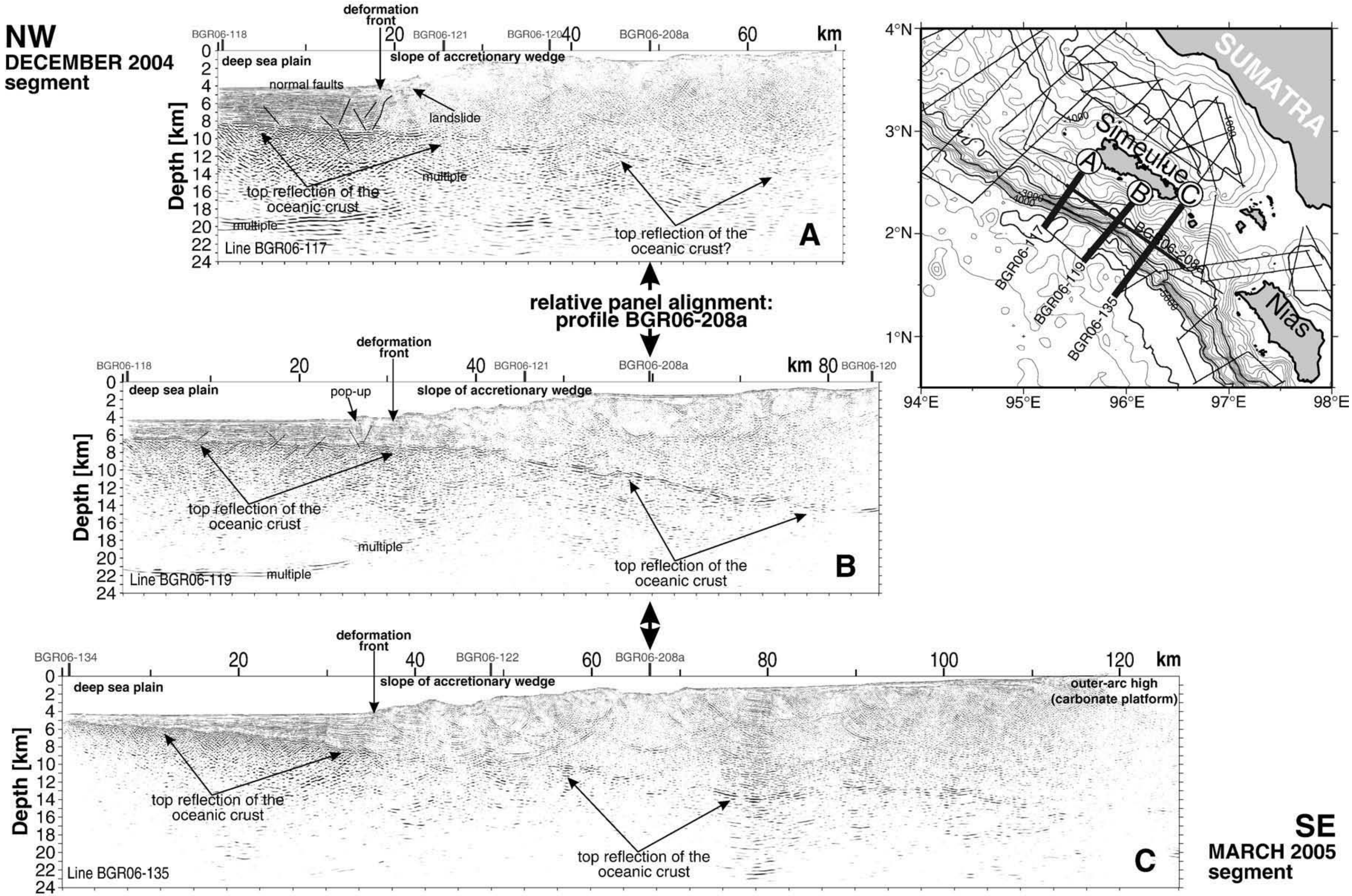

Fig. 4. Three prestack-depth migrated multichannel seismic lines crossing the accretionary prism west and south of Simeulue Island (BGR06-117, -119, -135) show that the variations in the topography of the oceanic crust coincide with a change in the structural style of the accretionary wedge and that the intersection of the dip lines with the margin-parallel line is 34 ± 2 km landward of the toe of the accretionary prism. Relative panel alignment is along the margin-parallel line BGR06-208a (Fig. 3). The locations of the profiles are indicated as thick purple lines in Fig. 1. The northern line BGR06-117 (A) is in the December 2004 segment. In the trench the gentle dipping oceanic crust is covered by a thick sedimentary pile (>4 km) and the accretionary prism has a steep outboard slope. The line in the centre BGR06-119 (B) also has a gently dipping oceanic crust beneath the frontal accretionary prism but mainly exhibits a structural high in the oceanic crust beneath the trench. The top of the oceanic crust is 7 km deep in the west and at about 7.8 km beneath the slope. The southern line BGR06-135 (C) bisects the broad re-entrant along the Sunda Arc. The trench fill is strongly wedge-shaped, thickening from 1 km to 4 km at the deformation front. The dip of the oceanic plate increases and thrusts in the accretionary prism form steeply dipping, seaward verging, antiformal stacked slices. The small map shows the location of the multichannel seismic profiles.

Southeast of 2°N (Fig. 3 — bottom; profile km 70) there are no MCS reflections from the top of the oceanic crust for some 20 km. This absence of reflections is where, on the wide-angle seismic data, there is a gradual increase in depth of the oceanic crust. Further south at km 45 on the MCS line, the oceanic crust reappears as a weak, discontinuous reflection about 2 km deeper than in the central part of profile. The change in reflectivity is not due to any change in the character of the overlying sediments because these can be traced across this region.

In the region traversed by the seismic line the deformation front is slightly curved because it is located in the broad re-entrant region between Nias and Simeulue islands. However, the change in the depth of the oceanic crust cannot be attributed to an oblique relationship between the orientation of the seismic line and the deformation front. Even if there was some limited obliquity between the orientation of the seismic line and the dip of the slab, given an average dip of the oceanic crust of about 5° an offstrike distance of 2 km either up or down the slab would result in a depth change of the top oceanic crust of less than 200 m.

From both seismic datasets we can identify an increase in depth along the strike of the oceanic crust of between 2 km (MCS) and 3 km (wide-angle data). Due to the MCS streamer length of 3000 m, absolute oceanic crust depth values are probably better resolved from the wide-angle seismic data. The observed variations in slab depth are due to a prominent structural relief in the lower plate. The location of the change in slab depth coincides with the segment boundary outlined by the aftershock distribution (Ammon, 2006). The depth change is limited to a 40 km wide region of the lower plate at approximately 2°N and 96°E.

4.2. Structural architecture and domains along the margin

Southwest of Simeulue, towards the trench, we acquired MCS data along three dip lines that cross the accretionary prism. These lines are shown in Fig. 4 arranged relatively to the line-ties with BGR06-208a.

Profile BGR06-117 (Fig. 4A) is located in the southern region of the December 2004 earthquake rupture. The line extends for some 72 km across the trench and accretionary prism at the northwestern tip of the re-entrant. Along the line the trench fill is more than 4 km (3.4 s TWT) thick and at the seabed completely levels out the oceanic crust relief. The fill consists of continuous parallel to sub-parallel reflections cut by palaeo-channels. The seismic character is typical of turbidite facies. A series of conjugate normal faults cuts the entire trench fill. The oceanic crust can be traced beneath the frontal accretionary prism. It dips at about 4°. At the tie-point with line BGR06-208a, some 34 km northeast of the toe of the accretionary prism, the oceanic crust is at a depth of ~12.5 km. Almost all the sedimentary cover on the incoming plate is offscraped and deformed at the prism toe. Thus almost all incoming sediment is accreted to the frontal prism. Within 12 km of the prism toe there is a doubling of the sediment thickness resting on the subducting plate. This increase in sediment thickness results in an extraordinarily steep prism slope of 15°. The increase in thickness is accompanied by frontal collapse structures.

MCS line BGR06-119 is located 60 km to the SSE of BGR06-117, just offshore and perpendicular to Simeulue Island. At the southwest end of the line, the top of the oceanic crust is at 7 km depth. Beneath the prism toe this depth increases to about 8 km (Fig. 4B). Oceanic crust depths are considerably shallower (~2 km) than on line BGR06-117 (Fig. 4A). Along line BGR06-119 the oceanic crust entering the subduction zone shows a similar normal fault pattern to that on line BGR06-117. However, the trench fill is only 2 km thick and slightly more wedge-shaped as it passes towards the accretionary prism. Normal faults penetrate the trench fill but heal upwards. Above a 500 m elevated graben shoulder in the oceanic crust a popup structure delineates the youngest outboard deformation. Again, there is frontal accretion of almost the whole trench fill at the prism toe, thus the incoming sediments are basally detached. However, the resulting frontal toe of the accretionary wedge is broader than further north and not as steeply dipping. The oceanic crust dips gently beneath the trench at the toe but the dip increases beneath the slope. About 32 km from the toe of the prism it reaches a depth of ~11.5 km at the line-tie with line BGR06-208a. Here the oceanic crust dips of ~6°.

MCS line BGR06-135 runs from SW to NE from the oceanic plate to the eastern part of the Simeulue Basin (Fig. 4C). It is located in the northern region of the March 2005 rupture. The profile lies at the apex of the broad re-entrant located off of Simeulue and Nias Island. The trench fill is strongly wedge-shaped, thickening from 1 km in the southwest to 4 km at the deformation front. Again, the trench fill and oceanic crust are normally faulted. In the lower section of the accretionary prism there is imbricate thrusting of the accreted sediment similar in style to that on line BGR06-119 and also seen further south (Schlüter et al., 2002; Susilohadi et al., 2005). The oceanic crust reflection is discontinuous but can be traced for more than 70 km to the northeast of the deformation front (Fig. 4C). There is an increase in depth of the oceanic crust from 9 km at the deformation front to ~13 km at the line-tie with line BGR06-208a. This corresponds to a slab dip of 6.7° beneath the frontal accretionary prism.

Comparing the three cross-profiles we establish an increase in slab dip from the north (4°) to the south (6.7°) beneath the frontal prism slope. This trend is accompanied by decreasing seabed slope angle of the frontal accretionary prism. Large seabed slope angles in the north coincide with the accretion of a thick sedimentary column whereas the thinner incoming sedimentary pile south of Simeulue Island corresponds with lower slope angles.

5. Discussion

5.1. Origin of slab relief

The simplest hypothesis to explain the shallow depth oceanic slab north of 2° identified on our data, would be a broad rise on the lower plate created as the Indo-Australian Plate is subducted beneath the 300 km long re-entrant. The re-entrant (Fig. 1) extends as far south as Nias Island and interaction with the overriding Eurasian plate along this feature would result in a rise in the oceanic plate with the apex approximately located midway between Nias and Simeulue islands. However, there are several inconsistencies in this explanation that lead us to consider a different source to be more likely. Our seismic profiles show that the shallowest slab reflections are in the northern third of the re-entrant, offshore of Simeulue. The shallow slab section here is only 60 km long and the dips at either end resolved by our data are too steep to be explained by a rise of longer (300 km) wavelength. The opposing dip directions at the ends of the slab suggest a smaller, more local, source. Moreover, on line BGR06-135, located at the apex of the re-entrant, there is an oceanic crust that is more steeply landward dipping (Fig. 4C) than to the north (Figs. 4A and B). This would not be expected if the shallow slab was formed by a broad rise on oceanic crust

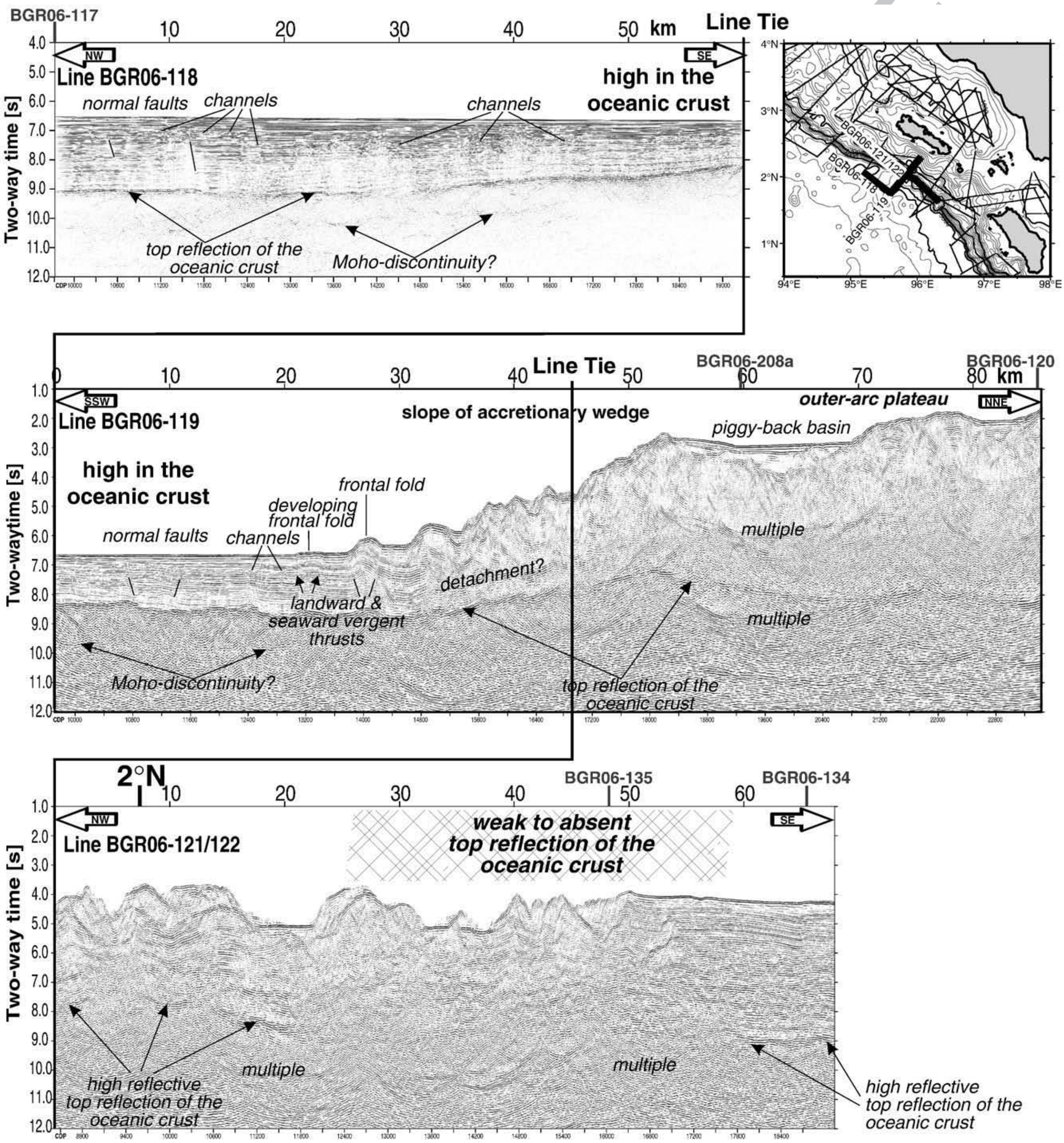

Fig. 5. Time migrated seismic sections from the trench and frontal slope of the accretionary prism. Line BGR06-118 (top) runs margin parallel in the trench SW of Simeulue Island. The oceanic basement shallows remarkably from 9.1 s (TWT) in the NW to 8.25 s (TWT) in the SE, at the intersection with line BGR06-119. Along line BGR06-119 landward and seaward verging thrusts at the deformation front and a fully developed frontal fold are developed. The composite line BGR06-121/122 runs in strike with the slope and shows a pointed depth variation in the subducting oceanic crust from 7.8 s (TWT) in the NW to 9.0 s (TWT) about 70 km to the SE. Both locations are about 20 km landward of the toe of the accretionary prism. At both ends of the line the top oceanic crust reflection is highly reflective while the reflection becomes weak to absent in the centre (profile km 26–58).

Please cite this article as: Franke, D., et al., The great Sumatra–Andaman earthquakes — Imaging the boundary between the ruptures of the great 2004 and 2005 earthquakes, Earth Planet. Sci. Lett. (2008), doi:10.1016/j.epsl.2008.01.047

subducting along the re-entrant. We conclude, therefore, that the narrow width and steep marginal dips of the shallow slab reflection cannot be explained by a broad rise on the slab that has formed by broad-scale subduction beneath the re-entrant. Rather, the data support the subduction of an elongated, narrow high on the subducting plate.

For the origin of the narrow high we refer to the Indo-Australian Plate offshore of Sumatra, the structure of which is reasonably well established (Cande et al., 1989; Deplus et al., 1998; Milsom, 2005; Delescluse and Chamot-Rooke, 2007). Dominant structures on the plate are E–W trending extinct spreading ridges, or N–S trending fracture zones. However, on the oceanic plate off Simeulue Island along strike from the feature we identify, neither spreading ridges nor fracture zones are evident on our high-resolution bathymetry nor on satellite altimetry (Smith and Sandwell, 1997). Further south, where the sedimentary cover thins, several fracture zones are imaged on gravity and magnetic data and the satellite altimetry (Smith and Sandwell, 1997). Morphologically, these fracture zones appear as complex structures of alternating topographic highs and lows (Ladage et al., 2006). Their width (30–50 km) and relief (~500–2000 m) are of same order of magnitude as the rise observed in our seismic data south of Simeulue. The Investigator Fracture Zone, which trends approximately north–south at 98°E, has an estimated elevation of up to 2000 m (Milsom, 2005).

North of the re-entrant, at 93.2°E and 93.6°E, Sibuet et al. (2007) propose that north–south oriented tectonic lineaments on the incoming plate are related to palaeo-fracture zones. These authors suggest that these fracture zones have been subducted and are influencing upper plate deformation, being reactivated with left-lateral slip during the December 2004 mainshock. Another fracture zone, further south of those identified by Sibuet et al. (2007), can also be mapped from magnetic anomaly patterns (Cande et al., 1989; Barckhausen, 2006) and traced into the area off Simeulue. A fracture zone at this location was also inferred by Newcomb and McCann (1987). It projects almost exactly onto the location of the elevated oceanic crust we identify along line BGR06-208a (Fig. 3). In conclusion, we suggest that it is this fracture zone, now deeply buried beneath trench sediment, that is the source of the shallow flat slab we identify on line BGR06-208a.

5.2. Orientation of shallow slab/fracture zone

The question remains, what is the orientation of the shallow slab, and does this support a fracture zone origin? Fig. 3 shows a slightly NW dipping oceanic crust reflection in the NW part of line BGR06-208a. As this is at the edge of the velocity–depth model, the increase in depth of the oceanic crust to the NW is not well constrained. However, in this region, but further to the southwest on line BGR06-118 (Fig. 5 — top) we observe a similar depth trend in the oceanic crust seaward of the accretionary prism. Seismic line BGR06-118 is about 60 km SW of the prism toe and oriented parallel to the trench as well as to line BGR06-208a. The top of the oceanic crust is well imaged and dips to the NW, as on line BGR06-208a. It shallows over a distance of 30 km from 9.1 s (TWT) in the NW to 8.25 s (TWT) in the SE (Fig. 5 — top) where it intersects line BGR06-119 (Fig. 5 — middle). Its relief at seabed is masked by the drape of the trench fill sediments. A line connecting the relief in the oceanic crust identified along line BGR06-118 with the increase in depth of the oceanic crust to the NW along the margin-parallel line BGR06-208a would strike NNE.

Turning to composite line BGR06-121/122 (Fig. 5 — bottom). This line is margin parallel and located between the toe of the accretionary prism and line BGR06-208a. At the cross tie between lines BGR06-119 and BGR06-121/122 the oceanic crust is at a depth of 7.8 s (TWT). At the southern end of BGR06-121/122, about 70 km to the south, it is at 9.0 s (TWT) (Fig. 5, bottom). The sedimentary thickness is 4 s (TWT) at the northwestern end of the line whereas it is up to 5 s (TWT) in the southeast. Although the seabed relief is more irregular in the northwest (smoother in the southeast) the water depths on average remain the same along the line. However, although the top oceanic crust reflection is clearly imaged at both ends of the line, between km 25 and 58 it disappears. Both locations are about 20 km landward of the toe of the accretionary prism. In the SE part of the profile the back limb of an anticline is imaged showing smooth topography and subhorizontal strata. It is therefore surprising that the highly reflective top oceanic crust reflection becomes weak to absent northeast of km 58, where it still underlies the subhorizontal strata (Fig. 5 — bottom).

We consider the absence of the reflection to be attributable to the same cause as on line BGR06-208a. Allowing for the difference in sediment thickness along line BGR06-121/122, that would result in a velocity pull-up in the southeast, in the southeast the oceanic crust reflection is about 2.5 km deeper than in the northwest. A line connecting the locations of weak oceanic crust reflections as well as the increase in depth from composite line BGR06-121/122 and line BGR06-208a would strike NNE towards Simeulue (Fig. 6 — top).

5.3. Links between lower and upper plates

GPS measurements on Simeulue Island (Subarya et al., 2006, Briggs et al., 2006) reveal vertical uplift in the north during the earthquake of December 2004 and uplift in the south of the island during the March 2005 event. The differential uplift defines a saddle in the middle of the island. It is taken as evidence for a major basement structure that may control rupture termination and a segment boundary (Briggs et al., 2006). Projecting the trend of the slab rise (fracture zone) on our seismic data onto Simeulue Island reveals a close alignment with the saddle identified by Briggs et al. (2006), with a trend of NNE–SSW (~N10°). The proposed NNE trend identified on our data also projects onto the nucleation point of the December 2004 earthquake (Fig. 6 — top). Consideration of the uplift on Simeulue in the context of our interpretations of an increase in depth of the oceanic crust seen in our wide-angle/refraction and MCS data may reflect a common cause.

Relative plate convergence between the Indo-Australian and Eurasian plates is parallel to the general trend of the strike of the extinct fracture zones (Subarya et al., 2006; Simons et al., 2007). Assuming a constant plate motion vector for the past 5

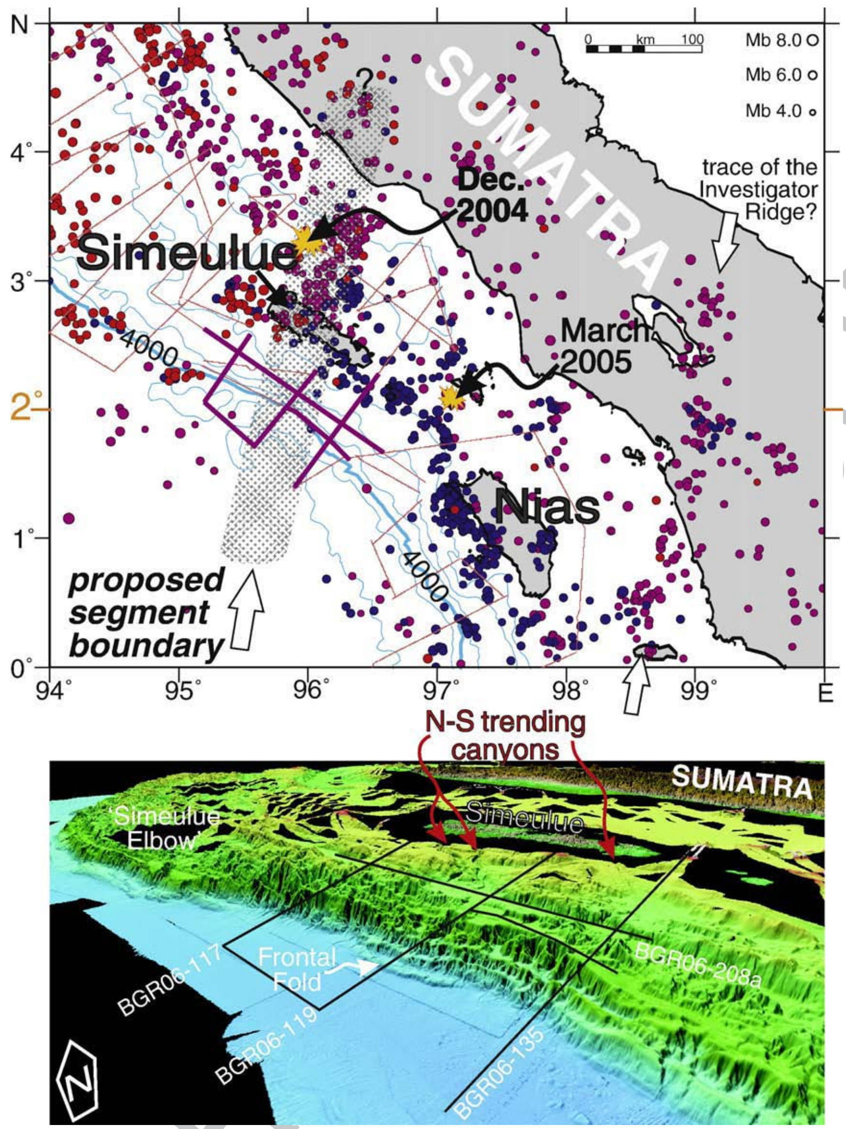

Fig. 6. NNE extent of the proposed segment boundary as revealed by the seismic data (upper panel) and enlarged bathymetric map of the broad re-entrant south of Simeulue Island (lower panel). Top: Seismicity before December, 26th 2004 is shown in purple, aftershocks of the 2004 mainshock in red, and aftershocks of the 2005 mainshock in blue (Engdahl et al., 2007). The distribution of the earthquakes is not in contradiction to the proposed trend of the segment boundary. The likely trace of the subducting Investigator Ridge indicated by an elongated cluster of epicentres is also marked. Purple lines mark the location of the reflection seismic lines shown in Figs. 3, 4 and 5. Bottom: Swath bathymetry shown with a vertical exaggeration of 2. Location of the seismic lines discussed in the text is indicated. The slope off Simeulue Island is cut by canyons striking N–S, probably linked to structures of the subducting plate, most likely a fracture zone. (For interpretation of the references to colour in this figure legend, the reader is referred to the web version of this article.)

million years (Hall, 2002; Delescluse and Chamot-Rooke, 2007) the location of the collision between an N–S oriented fracture zone and the convergent margin has remained stationary. This coincidence between the relative plate vector and the strike of the extinct fracture zones results in the deformation of the upper plate during subduction of the fracture zone ridge remaining stationary also. It is surmised that such deformation over an extended time period would produce a significant structural change in the over-riding plate, such as a major tectonic boundary. There appears to be no large-scale evidence of this structural change on Simeulue Island, nor on the accretionary prism. However, offshore of Simeulue Island, to the southwest, there are several submarine canyons. These canyons are aligned with tectonic lineaments striking N–S (Fig. 6 — bottom; Ladage et al., 2006). They may be an expression of local tectonic deformation due to the deformation identified on our seismic data and on Simeulue. Their presence may reflect a pervasive structural control by the oceanic plate on upper plate deformation. Therefore, we propose that off Simeulue the structural relief of a subducting extinct fracture zone entering the accretionary wedge at about 2°N contributes to or is a major control on segmentation of the forearc. DeShon et al. (2005) suggest that the southern boundary of the Andaman microplate is located in the vicinity of Simeulue Island. Although the evidence is equivocal, it may also be that this boundary was initiated by subduction of the fracture zone.

However, the evidence suggests that NNE–SSW oriented fracture zones on the oceanic plate are influencing deformation

Please cite this article as: Franke, D., et al., The great Sumatra–Andaman earthquakes — Imaging the boundary between the ruptures of the great 2004 and 2005 earthquakes, Earth Planet. Sci. Lett. (2008), doi:10.1016/j.epsl.2008.01.047

on the over-riding plate, imparting structures that are oriented in the same direction. Previously, the orientation of the segment boundary was inferred to be orthogonal to the plate boundary (Newcomb and McCann, 1987; Ammon et al., 2005; Bilham, 2005). In this regard the aftershock distribution is ambiguous but, however, in terms of orientation of the segment boundary, does not discount an alternative trend of NNE–SSW (Fig. 6).

5.4. Simeulue segment boundary

Fracture zones and other structural discontinuities on the downgoing plate are first-order candidates for the initiation of segmentation and earthquake rupture termination between the 2004 and 2005 earthquakes (e.g. Subarya et al., 2006). Our data lends support to this interpretation. The shallow slab we identify is 60 km wide and elevated for about 1 km towards the NW and for some 3 km towards the SE. As an extinct fracture zone, it is comparable in width and height, to the Investigator Ridge, another N–S trending fracture zone on the Indo-Australian Plate. Located further south, the Investigator Ridge, where it collides with the accretionary wedge at 89°E, 2.5°S, has a width of 30–50 km and an elevation of about 1 km. Perhaps significantly, the collision zone of this feature correlates with the boundary between the 1797 and 1833 great earthquakes (northern end) and the 1861 great earthquake (southern end) offshore of southern Sumatra (Fauzi et al., 1996; Sieh and Natawidjaja, 2000; Rivera et al., 2002).

A particular feature of the Simeulue fracture zone that may contribute to its effect on margin segmentation is its size and asymmetry. The relief of the fracture zone is far greater than that of the other prominent fracture zones and ridges (including the Investigator Ridge) on the Indo-Australian plate. The eastern flank of the ridge off Simeulue is at 3 km high much higher than the western flank. This height is twice that of the Investigator Ridge.

This relief across a fracture zone could be a function of the juxtaposition of crust of significantly different ages. The general age of the oceanic crust, however, is Eocene and, assuming symmetrical spreading, there is an age difference of ~2 Ma (Cande et al., 1989). The resulting seafloor depth difference will, therefore, be only of the order of 100–200 m, a difference that cannot account for the overall relief observed across the fracture zone.

Alternatively a fault or tear at the eastern flank of the proposed fracture zone could explain the depth difference of 3 km we observe. Modelling the wide-angle seismic data reveals that the top of the subducting oceanic crust gradually increases in depth (Fig. 3 — top). However, the spatial resolution is limited due to the layout of the wide-angle seismic experiment and the modelling algorithm used. An abrupt depth change like a steep ramp or tear would also be resolved as smooth transition with this acquisition configuration.

The interpretation of this feature as a fault or tear is supported by the MCS data. These show weak and discontinuous reflections on both margin-parallel lines BGR06-208a and BGR06-122 east of the topographic high of the proposed fracture zone (Figs. 3 and 5). This reflection character would not be expected if it were merely a gradual change in slab depth. Rather, it favours a faulted and dissected eastern flank of the Simeulue fracture zone.

The N–S to NNE–SSW striking fracture zones on the Indo-Australian plate between the Ninetyeast ridge and Sumatra are activated and reactivated as left-lateral strike-slip faults (Deplus et al., 1998). Close to the trench these are additionally reactivated as normal faults caused by flexural bending of the oceanic plate as it descends into the subduction zone (Schauer et al., 2006; Graindorge et al., 2007). The fracture zone off of Simeulue we consider to be similarly reactivated and dip-slip movements along the eastern flank have resulted in the observed step in the oceanic slab. Faulting along the eastern edge of this fracture zone possibly penetrates the entire oceanic slab. The result could be a tear in the subducting plate as slab dip increases beneath the accretionary prism. This may be an answer, as to why the Simeulue fracture zone is such a prominent barrier to rupture propagation.

6. Conclusions

Interpretation of a suite of marine geophysical data including wide-angle seismic and multichannel reflection seismic reveals a ridge on the subducting oceanic crust, entering the accretionary wedge off Sumatra located at 95.6°E, 2°N. The western flank of the ridge is about 1 km high whereas the eastern flank is up to 3 km. Trench sediments up to 5 km in thickness mask the topographic relief of the oceanic crust so that the ridge is not visible on the bathymetric data. The ridge is about 60 km wide and strikes in NNE–SSW direction. It extends beneath the accretionary wedge and likely also beneath Simeulue Island.

The projection of the ridge beneath the accretionary wedge and further under the forearc basins plots onto the common segment boundary of the 2004 and 2005 mainshocks. This relationship implies a structural control of the downgoing ridge on the segment boundary between the huge ruptures of the December 2004 and the March 2005 earthquakes. The trend of the ridge is parallel to fracture zones on the Indo-Australian plate and we consider such a fracture zone, buried by thick sediments as likely origin of the ridge.

The ridge on the oceanic crust contributes to or is a major control on the initiation of the segment boundary. The step in the slab across the eastern flank of the proposed ridge/fracture zone could be the result of either a gradual, oblique ramp or a shallow slab tear. However, the gradual depth change of 3 km as derived by wide-angle/refraction seismic data coincides with a significant change in the reflectivity of the oceanic crust reflection in the multichannel seismic data. We consider that this may reflect a dissected and faulted subducting oceanic crust. Dip-slip movements along the eastern flank of the subducting fracture zone beneath Simeulue may be considered as intensification factor in terms of rupture propagation barrier.

Acknowledgements

We are indebted to the Government of Indonesia (BPPT) as Indonesian partner providing the permission for the investigations in its territorial water. We thank ship's masters and their crew for operating RV Sonne. We are grateful to Petrologic

Geophysical Service Gmbh, Hannover, Germany for providing support in performing the prestack-depth migration. The SASS multibeam data was acquired by HMS SCOTT, a UK Royal Navy Survey Vessel during Marine Scientific Research coordinated by the Joint Environment Directorate of Defence Intelligence, and the data was processed by the United Kingdom Hydrographic Office. David Tappin publishes with the permission of the Executive Director of the British Geological Survey. We thank Robert Engdahl for providing hypocentre data. Helpful comments by two anonymous reviewers are kindly acknowledged. The German Ministry for Research and Education (BMBF) supported the study (grants 03G0186A and 03G0189A). This is publication no. 2 of the SeaCause project.

Appendix A. Supplementary data

Supplementary data associated with this article can be found, in the online version, at doi:10.1016/j.epsl.2008.01.047.

References

Aki, K., 1979. Characterization of barriers on an earthquake fault. J. Geophys. Res. 84, 6140–6148.

Ammon, C.J., 2006. Megathrust investigations (News and Views). Nature 440 (7080), 31–32.

Ammon, C.J., Ji, C., Thio, H.-K., Robinson, D., Ni, S., Hjorleisdottir, V., Kanamori, H., Lay, T., Das, S., Helmberger, D., Ichinose, G., Polet, J., Wald, D., 2005. Rupture process of the 2004 Sumatra–Andaman earthquake. Science 308, 1133–1139.

Ando, M., 1975. Source mechanisms and tectonic significance of historical earthquakes along the Nankai Trough, Japan. Tectonophysics 27, 119–140.

Barckhausen, U., 2006. The segmentation of the subduction zone offshore Sumatra: relations between upper and lower plate. EOS Trans. AGU 87 ((52), Fall Meet. Suppl.), U53A–0029.

Baroux, E., Avouac, J.-P., Bellier, O., Sébrier, M., 1998. Slip-partitioning and fore-arc deformation at the Sunda-Trench, Indonesia. Terra Nova 10 (3), 139–144.

Bilek, S.L., Schwartz, S.Y., DeShon, H.R., 2003. Control of seafloor roughness on earthquake rupture behaviour. Geology 31, 455–458.

Bilham, R., 2005. A flying start, then a slow slip. Science 308, 1126–1127.

Briggs, R.W., Sieh, K., Meltzner, A.J., Natawidjaja, D., Galetzka, J., Suwargadi, B., Hsu, Y.-J., Simons, M., Hananto, N., Suprihanto, I., Prayudi, D., Avouac, J.-P., Prawirodirdjo, L., Bock, Y., 2006. Deformation and slip along the Sunda megathrust in the great 2005 Nias–Simeulue earthquake. Science 311, 1897–1901.

Cande, S.C., LaBrecque, J.L., Larson, R.L., Pitman, W.C., Golovchenko, X., Haxby, W.F., 1989. Magnetic Lineations of the World's Ocean Basins. LDGO Contribution 4367. AAPG, Tulsa, Oklahoma.

Collot, J.-Y., Marcaillou, B., Sage, F., Michaud, F., Agudelo, W., Charvis, P., Graindorge, D., Gutscher, M.-A., Spence, G., 2004. Are rupture zone limits of great subduction earthquakes controlled by upper plate structures? Evidence from multichannel seismic reflection data acquired across the northern Ecuador–southwest Colombia margin. J. Geophys. Res. 109, B11103. doi:10.1029/2004JB003060.

Cummins, P.R., Baba, T., Kodaira, S., Kaneda, Y., 2002. The 1946 Nankai earthquake and segmentation of the Nankai Trough. Phys. Earth Planet. Inter. 132, 75–87.

Delescluse, M., Chamot-Rooke, N., 2007. Instantaneous deformation and kinematics of the India–Australia Plate. Geophys. J. Int. 168 (2), 818–842. doi:10.1111/j.1365-246X.2006.03181.x.

DeShon, H.R., Engdahl, E.R., Thurber, C.H., Brudzinski, M., 2005. Constraining the boundary between the Sunda and Andaman subduction systems: evidence from the 2002 Mw 7.3 Northern Sumatra earthquake and aftershock relocations of the 2004 and 2005 great earthquakes. Geophys. Res. Lett. 32, L24307. doi:10.1029/2005 GL024188.

Deplus, C., Diament, M., Hebert, H., Bertrand, G., Dominguez, S., Dubois, J., Malod, J., Patriat, P., Pontoise, B., Sibilla, J.-J., 1998. Direct evidence of active deformation in the eastern Indian oceanic plate. Geology 26, 131–134.

Dewey, J.W., Benz, H., Choy, G., Earle, P., Presgrave, B., Sipkin, S., Tarr, A.C., Wald, D., 2007. Seismicity associated with the Sumatra–Andaman Islands earthquake of 26 December 2004. Bull. Seismol. Soc. Am. 97 (1A), 25–42.

Engdahl, E.R., Villasenor, A., DeShon, H.R., Thurber, C., 2007. Teleseismic relocation and assessment of seismicity (1918–2005) in the region of the 2004 Mw 9 Sumatra–Andaman and 2005 M 8.7 Nias great earthquakes. Bull. Seismol. Soc. Am. 97, 43–61. doi:10.1785/0120050614.

Fauzi, F., McCaffrey, R., Wark, R.D., Sunaryo, P.Y., Haryadi, P., 1996. Lateral variation in slab orientation beneath Toba Caldera, northern Sumatra. Geophys. Res. Lett. 23, 443–446.

Gahalaut, V.K., Nagarajan, B., Catherine, J.K., Kumar, S., 2006. Constraints on 2004 Sumatra–Andaman earthquake rupture from GPS measurements in Andaman–Nicobar Islands. EPSL 242, 365–374.

Graindorge, D., Klingelhoefer, F., Gutscher, M.-A., Sibuet, J.-C., McNeill, L., Henstock, T., Dean, S., Tappin, D., Dessa, J.-X., Singh, S., 2007. Lower plate control of upper plate deformation at the toe of the NW Sumatra convergent margin from swath bathymetry. Geophys. Res. Abstr. 9, 05979 SRef-ID: 1607-7962/gra/EGU2007-A-05979.

Hall, R., 2002. Cenozoic geological and plate tectonic evolution of SE Asia and the SW Pacific: computer-based reconstructions, model and animations. J. Asian Earth Sci. 20 (4), 353–431.

Henstock, T.J., McNeill, L.C., Tappin, D.R., 2006. Seafloor morphology of the Sumatran subduction zone: surface rupture during megathrust earthquakes? Geology 34, 485–488.

Kamesh Raju, K.A., Murty, G.P.S., Amarnath, Dileep, Kumar, M.L.M., 2007. The west Andaman fault and its influence on the aftershock pattern of the recent megathrust earthquakes in the Andaman–Sumatra region. Geophys. Res. Lett. 34, L03305. doi:10.1029/2006GL028730.

Kodaira, S., Takahashi, N., Nakanishi, A., Miura, S., Kaneda, Y., 2000. Subducted seamount imaged in the rupture zone of the 1946 Nankaido earthquake. Sciences 289, 104–106.

Korenaga, J., Holbrook, W.S., Kent, G.M., Kelemen, P.B., Detrick, R.S., Larsen, H.-C., Hopper, J.R., Dahl-Jensen, T., 2000. Crustal structure of the southeast Greenland margin from joint refraction and reflection seismic tomography. J. Geophys. Res. 105, 21591–21614.

Krüger, F., Ohrnberger, M., 2005. Tracking the rupture of the Mw = 9.3 Sumatra earthquake over 1,150 km at teleseismic distance. Lett. Nature. doi:10.1038/nature03696.

Ladage, S., Gaedicke, C., Barckhausen, U., Heyde, I., Weinrebe, W., Flueh, E.R., Krabbenhoeft, A., Kopp, H., Fajar, S., Djajadihardja, Y., 2006. Bathymetric survey images structure off Sumatra. EOS Trans. AGU 87 (17), 165.

Lay, T., Kanamori, H., Ammon, C.J., Nettles, M., Ward, S.N., Aster, R.C., Beck, S.L., Bilek, S.L., Brudzinski, M.R., Butler, R., DeShon, H.R., Ekström, G., Satake, K., Sipkin, S., 2005. The Great Sumatra–Andaman earthquake of 26 December 2004. Science 308, 1127–1133.

McCarthy, A.J., Elders, C.F., 1997. Cenozoic deformation in Sumatra: oblique subduction and the development of the Sumatran Fault System. In: Fraser, A.J., Matthews, S.J., Murphy, R.W. (Eds.), Petroleum Geology of Southeast Asia. Geol. Soc. Spec. Publ., vol. 126, pp. 355–363.

Malod, J.A., Kemal, B.M., 1996. The Sumatra margin: oblique subduction and lateral displacement of the accretionary prism. In: Hall, R., Blundell, D. (Eds.), Tectonic Evolution of Southeast Asia. Geol. Soc. Spec. Publ., vol. 106, pp. 19–28.

Milsom, J., 2005. Seismology and neotectonics (Chapter 2). In: Barber, A.J., Crow, M.J., Milsom, J.S. (Eds.), Sumatra. Geol. Soc. Mem, vol. 31, pp. 8–15.

Mooney, W.D., Brocher, T.M., 1987. Coincident seismic reflection/refraction studies of the continental lithosphere: a global review (paper 6R0778). Rev. Geophys. Space Phys. 25, 723–742.

Newcomb, K.R., McCann, W.R., 1987. Seismic history and seismotectonics of the Sunda arc. J. Geophys. Res. 92, 421–439.

Rivera, L., Sieh, K., Helmberger, D., Natawidjaja, D., 2002. A comparative study of the Sumatran subduction-zone earthquakes of 1935 and 1984. Bull. Seismol. Soc. Am. 92, 1721–1736.

Please cite this article as: Franke, D., et al., The great Sumatra–Andaman earthquakes — Imaging the boundary between the ruptures of the great 2004 and 2005 earthquakes, Earth Planet. Sci. Lett. (2008), doi:10.1016/j.epsl.2008.01.047

Ryan, H.F., Scholl, D.W., 1993. Geologic implications of great interplate earthquakes along the Aleutian arc. J. Geophys. Res. 98, 22135–22146.

Schauer, M., Ladage, S., Weinrebe, W., Berglar, K., Krabbenhoeft, A., Flueh, E., Gaedicke, C., 2006. Morphotectonics of the Sumatra margin — analysis of new swath bathymetry. EOS Trans. AGU 87 (52), U53A–0033 Fall Meeting Supplement.

Schlüter, H.U., Gaedicke, C., Roeser, H.A., Schreckenberger, B., Meyer, H., Reichert, C., Djajadihardja, Y., Prexl, A., 2002. Tectonic features of the southern Sumatra–western Java fore-arc of Indonesia. Tectonics 21, 1047. doi:10.1029/2001TC901048.

Sibuet, J.-C., Rangin, C., Le Pichon, X., Singh, S., Cattaneo, A., Graindorge, D., Klingelhoefer, F., Lin, J.-Y., Malod, J., Maury, T., Schneider, J.-L., Sultan, N., Umber, M., Yamaguchif, H., "Sumatra aftershocks" team, 2007. 26th December 2004 great Sumatra–Andaman earthquake: co-seismic and postseismic motions in northern Sumatra. Earth Planet. Sci. Lett. doi:10.1016/j.epsl.2007.09.005.

Sieh, K., Natawidjaja, D., 2000. Neotectonics of the Sumatran fault, Indonesia. J. Geophys. Res. 105 (B12), 28295–28326.

Simandjuntak, T.O., Barber, A.J., 1996. Contrasting tectonic styles in the Neogene orogenic belts of Indonesia. In: Hall, R., Blundell, D. (Eds.), Tectonic Evolution of Southeast Asia. Geol. Soc. Spec. Publ., vol. 106, pp. 185–201.

Simons, W.J.F., Socquet, A., Vigny, C., Ambrosius, B.A.C., Haji Abu, S., Promthong, Chaiwat, Subarya, C., Sarsito, D.A., Matheussen, S., Morgan, P., Spakman, W., 2007. A decade of GPS in Southeast Asia: resolving Sundaland motion and boundaries. J. Geophys. Res. 112, B06420. doi:10.1029/2005JB003868.

Singh, S.C., et al., 2005. Sumatra earthquake research indicates why rupture propagated northward. EOS Trans. AGU 86 (48), 497.

Smith, W.H.F., Sandwell, D.T., 1997. Global seafloor topography from satellite altimetry and ship depth soundings. Science 277, 1957–1962.

Spence, W., 1977. The Aleutian are: tectonic blocks, episodic subduction, strain diffusion, and magma generation. J. Geophys. Res. 82, 213–230.

Subarya, C., Chlieh, M., Prawirodirdjo, L., Avouac, J.-P., Bock, Y., Sieh, K., Meltzner, A.J., Natawidjaja, D.H., McCaffrey, R., 2006. Plate-boundary deformation associated with the great Sumatra–Andaman earthquake. Nature 440, 46–51.

Susilohadi, S., Gaedicke, C., Ehrhardt, A., 2005. Neogene structures and sedimentation history along the Sunda forearc basins off southwest Sumatra and southwest Java. Mar. Geol. 219, 133–154.

Yáñez, G., Cembrano, J., 2004. Role of viscous plate coupling in the late Tertiary Andean tectonics. J. Geophys. Res. 109, B02407. doi:10.1029/2003JB002494.

Please cite this article as: Franke, D., et al., The great Sumatra–Andaman earthquakes — Imaging the boundary between the ruptures of the great 2004 and 2005 earthquakes, Earth Planet. Sci. Lett. (2008), doi:10.1016/j.epsl.2008.01.047